8th Biennial International Conference
& Exposition on Petroleum Geophysics

"HYDERABAD 2010"

P-143

Pore size distribution and Ultrasonic Velocities of compacted Na-montmorillonite clays

Utpalendu Kuila, Manika Prasad and Mike Batzle*
Colorado School of Mines, CO, USA Corresponding

Summary

The pore-size distribution of the shales is controlled by the clay content of the shales. The clays have extremely small grain size and high surface area. Na- Montmorrillonite clays obtained from Clay Mineral Society are compacted to obtain pellets of with different porosities. Gas adsorption experiment is carried on powder clays and compacted pellets to understand the evolution of poresize distribution. The results suggest a decrease in pore diameter with compaction. The ultrasonic velocities of the clays are measured and compared with reported value.

Introduction

Shale exhibits dual-porosity structure and has more complex pore-structure than that of sandstones and limestones. The predominant gas flow occurs through the interconnected fracture network system and this system is recharged by the gas flowing through the matrix. Shale matrix has predominantly micro- to meso-pores (pore-size below 50 nm as per IUPAC classification). Another unique aspect of these sediments is the high pore surface area to pore volume ratio. Clays are layered–sheet silicate minerals of extremely small grain size which contributes to the large surface areas. The gas molecules attach themselves to these large surface areas by adsorption.

Clay constitutes more than 50 % of shales. The matrix porosity and the pore size distribution of shales are mostly controlled by percentage of clays present in it. This study is focused on understanding the pore structure of clayey sediments and their evolution with depth. Also the influence of these pore structures on the physical and acoustic properties will be studied.

Previous Work

Katsube et al. (1992) studied the evolution of shale pore structure with compaction by analyzing shales from Beaufort-MacKenzie Basin and Scotian shelf. Unimodal pore size distribution was reported with the modal size decreasing from 200 nm to 10-20 nm with depth. At larger depth the modal size was around 0.5 to 10 nm. Similar unimodal size distribution was reported by Schettler et al. (1989). Bustin et al. (2008) reported bimodal pore-size distribution with modes at 10 nm range and the other around 10,000 nm range. Ewy and Morton (2009) also reported bimodal to unimodal pore-size distribution in the poresize distribution in shale pellets compacted at lab.

Experimental Procedure

i. Sample Preparation:

Na-montmorillonite powders (Swy-2), obtained from the repository of Clay Mineral Society, is artificially compacted using cold pressing techniques to make pellets (Figure 1). The pressure was increased at a very slow rate. The samples are put inside a split cube barrel. The inner surfaces of the barrels are coated with Teflon tapes which prevent sticking of charged clays with the walls during the pressing. This also helps in reducing the friction associated while pushing the sample out of the barrel and sample recovery is made simple. The clays are sieved through 325 mesh (45 m) screen prior to pressing. The powders are then pressed at different pressures to obtain pellets with different porosities. The minimum and the maximum load applied are 6000 psi and 14000 psi respectively. The pellets are named using the percentage content of clays and the pressure applied, e.g. sample NaM100-6K means the pellet is made from 100 % Na-

email: ukuila@mymail.mines.edu

Montmorillonite by applying 6000 psi of axial load. The porosities were calculated from the mass, volume and the grain density of the pellets are shown in Table 1 (Note the porosities are calculated from measured bulk density and reported grain densities 2.3 g/cc). Chips are made from pellets for the gas adsorption experiment

ii. Gas adsorption experiment:

The gas adsorption experiment using nitrogen as adsorbent is conducted on Micromeritics ASAP 2020 surface area

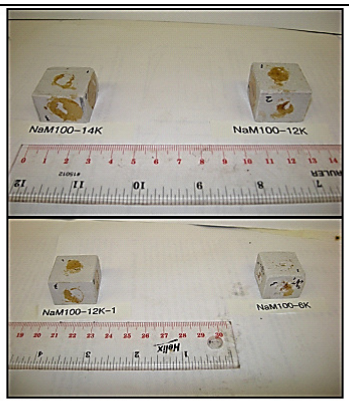

Figure 1: Cold Pressed Clay pellets samples obtained by compressing clay powder (Swy-2) at different axial loads. The acoustic couplant are seen on the face of these cubes.

analyzer. The gas absorption experiment is carried on three samples: powdered Swy-2 source Na-Montmorrilonite clays as obtained from Clay Mineral Society (NaM100-pw-US); Swy-2 clays sieved through 325 size mesh (grain size below 45 m) (NaM100-pw-Se) and clay pellet obtained from compressing sieved clay at 13000 psi (NaM100-13K). About 1 mg of sample is degassed at 130^{o}C from 6 hours under a vaccum of 10 mHg. This ensures removal of any bound and capillary water present. After degassing the sample, it is exposed to nitrogen gas near cryogenic temperature (-197.26^{o}C) at a series of precisely controlled pressures. Nitrogen adsorption volume are measured over the relative equilibrium adsorption pressure (P/Po) range of .05 -1. The gas adsorption isotherm is reported as the volume of gas adsorbed vs P/Po, where Po is the condensation pressure of nitrogen at laboratory conditions. At P/Po equal to 1, the entire gas is condensed to liquid inside the pores. Desorption experiment is carried by systematically reducing the pressure from the condensation pressure Po resulting in liberation of the adsorbed gas molecules. As with the adsorption process, the changing quantity of gas on the solid surface is quantified and reported as the desorption isotherm.

The surface area of the samples is measured by applying BET theory. BET theory suggests that there is a decrease in enthalpy of the adsorption from the first layer (mono-layer) to subsequent layers. This is manifested in the decrease in slope of the isotherm curve and distinguishes between mono-layer and multilayer vapor adsorption regime. The internal surface area is calculated from the volume of gas adsorbed to achieve monolayer coverage of pores (Schettler et.al 1989). The BET equation is a follows

$$x/[n(1-x)] = 1/n_m c + ((c-1)/n_m c)x$$

where x = P/Po, n is the volume of absorbate, n_m is the monolayer capacity and c is the constant related to heat of adsorption. By plotting the left term in the equation vs P/Po, the slope and the intercept gives expression to obtain nm and c. The plots should be taken in the P/Po range of monolayer adsorption (generally 0.05-0.20) identified by the break in the slope of isotherm as discussed earlier. The specific surface area is calculated using the value of nm obtained from the BET plot substituting in the following equation

$$S = n_m L a_m$$

where S is the surface area in m^2/gm, L is the Avogadro number (6.022 x 1023 mol^{-1}) and a_m is the area occupied by nitrogen molecule in a monolayer configuration (16.2 x 10-$^{20}m^2$).

The pore size distribution is obtained using Barett-JoynerHalenda (BJH) method. This theory uses Kelvin equation relating the radius of the liquid-vapor meniscus with the vapor pressure during capillary condensation through cylindrical pores. The BJH theory uses Kelvin equation and incorporates the effect of thinning of adsorbed layer through a reference isotherm (Schull 1948). At pressure Po (condensation pressure), the pores are completely filled with the condensed gas. With decreasing pressure, liquid evaporates out from the larger pore, as described by Kelvin equation and larger radius of meniscus. The isotherm at this pressure range will be governed the relative volumes of the particular pore-size and the pore size distribution can be obtained from the isotherm.

iii. Ultrasonic measurements:

Ultrasonic measurements of several compacted pellets are made to understand the acoustic effect of compaction. The ultrasonic P and S wave measurement are done by pulse transmission technique using a Panametrics tranducers. The ultrasonic measurements are made on all the three pairs of faces of the cube.

Results:

i. Adsorption isotherm, Surface area and Pore Size Distribution:

Figure 2 shows the typical isotherms for the sample NaM100-13K. The isotherms are Type II isotherms (as per IUPAC classification) typical for mesoporous substances. There is also a large hysteretic effect in the adsorption and the desorption curves. The hysteresis pattern is H3 (as per IUPAC classification) indicating presence of slit-like pores. (Condon 2006). Table 2 describes the different parameter calculated from the application of BET theory and BJH theory on the isotherm. The reported surface area for the Swy-2 (Dogan et a.l 2006) is much less than that obtained from analysis of this experiment [22.7 m^2/gm compared to 30.7 m^2/gm for NaM100-pw-US]. The surface area decreases between the sieved and the unseived powders. Its also decreases when compacted (the surface area for NaM100-13K is the less than the original sieved powder NaM100-pw-Se). The porosity for the range (17A – 3000 A) is calculated from the BJH pore volume calculation. The BJH theory gives the total volume of pore in cm3/gm and it is converted into porosity using a grain density of 2.3 gm/cc. The porosity is highest in the sieved powder and it decreases with compaction. Also the porosity values obtained are not equal is case for adsorption and desorption which may be the effect of the condensation in larger macro pores.

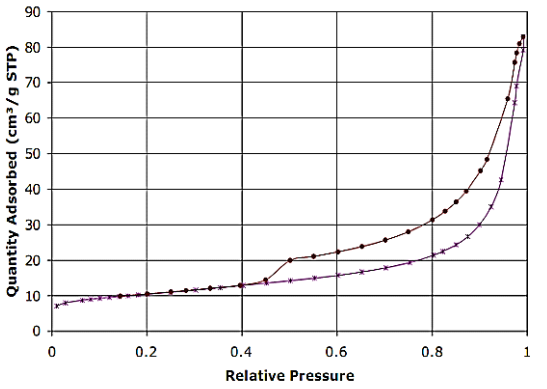

Figure 2. Nitrogen Adsorption -Desorption curve for NaM100-13K. The pink curve is the adsorption isotherm and the brown curve is the desorption isotherm. The relative pressure is the ratio of the absolute pressure to the condensation pressure of N_2.

Figure 3 and 4 shows the incremental pore size distribution (incremental pore volume vs pore diameter) obtained from the adsorption and desorption isotherm curve respectively. In case of the adsorption, the distribution is bimodal with a minor peak around 30-40 A. Another interesting observation is the change in the pore size distribution. There is no change in the

30-40 A peaks with different samples. The pore size distribution is entirely different in case of the desorption case. The pore size distributions have a major peak around 30-40 A.

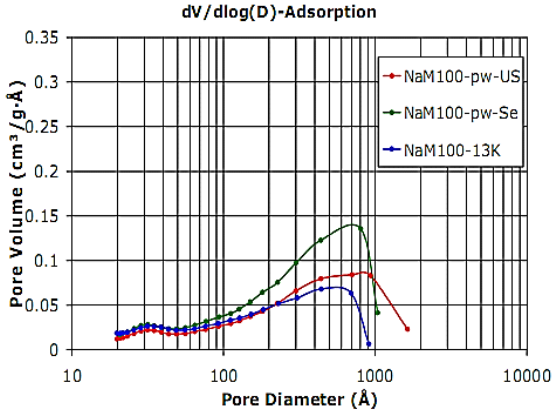

Figure 3: Adsorption pore size distribution for Swy-2 powder unsieved (red), Swy-2 powder sieved below 325 mesh (green) and NaM100-13K (blue)

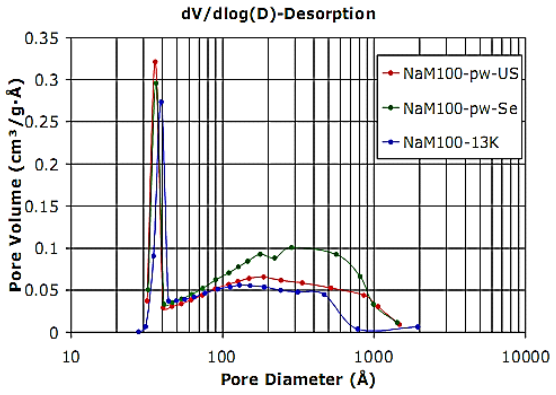

Figure 4: BJH desorption pore size distribution for Swy-2 powder unsieved (red), Swy-2 powder sieved below 325 mesh (green) and NaM100-13K (blue)

ii. Ultrasonic Velocities:

The ultrasonic measurements are made on all the three pairs of faces of the cube. The samples behave in transversely isotropic media i.e the velocities perpendicular to the compression direction are equal. Figure 5 and 6 shows the P-wave and the S-wave velocities respectively plotted as a function of porosity. Generally with decrease in porosity, the velocities increase, as expected. Sample NaM100-14K shows considerable lower Vpv and this may be due to some fractures. All the other velocities are slightly lower than the trend velocity indicating the sample may be cracked. Figure 7 and 8 respectively shows the Vp/Vs ratios and anisotropic parameters as a function of porosity. The horizontal Vp/Vs ratio or Vph/Vsh is relatively insensitive to porosity change.

Discussion:

i. Surface area and Pore Size Distribution:

The isotherm for the all the samples (two powders and one pellets) reveal that the majority of porosity is mesoporosity. This is with agreement from the observation of Dogan et. al 2006. The reason of the hysteresis is mostly due to the capillary condensation process in a heterogeneous pore structure. The adsorption and desorption are two different processes. During adsorption, multimolecular layers adsorption is followed by capillary condensation. During desorption capillary evaporation (liquid to gas) takes place. Capillary condensation starts from the narrowest pore during adsorption and capillary evaporation starts from the largest pore diameter. In heterogeneous pore network structure where smaller pores are connected to the larger pore, the adsorption will be a function of the direction i.e. whether the movement of the fluid is occurring from the larger to smaller pore or vice versa. Presence of heterogeneous pore structure is well documented in shales. Katsube et al. reported presence large storage pore connected with the smaller

connecting pore. Gas adsorption isotherm hysteresis may also occur for other reasons like pore blocking and difference in nucleation and evaporation sites in macropore. More work is necessary to understand the true nature of this hysteresis. Also in reservoir subsurface conditions the likelihood of the capillary condensation should be analyzed and incorporated in predicting whether we can see this hysteresis or not. The presence of this hysteresis has larger implications. The differences in the pore size distribution is case of adsorption and desorption indicate there will be a large difference in permeability as function of the direction of movement of the fluids. For example, in shale gas production the matrix flow will be essentially a desorption process and will different permeability as compared to adsorption. It will also impact the use of these isotherms in material balance calculations for shale gas which incorporates the effect of adsorption.

The pore size distribution shows bimodal size distribution; one mode at 30 Å and the other around 500 Å. The pore volume at 500 Å for the sieved one is more than the unsieved one. This can be explained by poor sorting of the later sediments and presence of coarser grains. As we compact the sediments the pore size distribution around 30 Å doesn't change but there is a reduction in the pore volume around 500 Å. This is due to compaction and better alignment of clays plates.

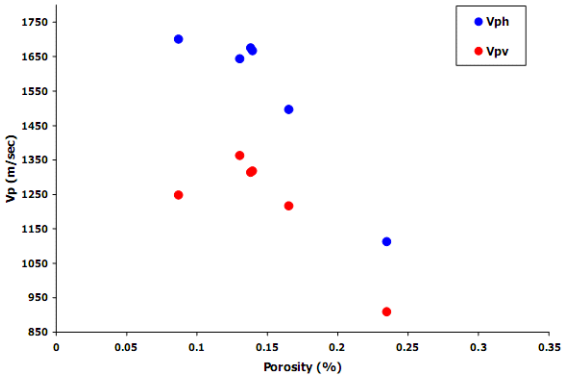

Figure 5: P-wave velocities as a function of porosity.

ii. Acoustic Velocities

Figure 9 and 10 shows the comparison of results in these studies with other studies published in the literature. The datasets used for the comparison are from Namontmorillonite measurement from Vanorio et al. (2003) measurements on clay-rich recent sediments containing about 35-40% clays (Kuila et. al., 2006) and from the measurements on Na-montmorillonite from Bandyopadhyay et. al. 2008. Our study shows a steeper trend in velocity – porosity space than reported by Bandyopadhyay (2008). However the trend is more or less comparable with the trends reported by Vanorio and Kuila. Kuila et al (2006) has higher velocities as their sample contains only 40 % clays. Vanorio's data have quite a bit of scatter but the values are in general lower than this study. This can be attributed to the humidity difference in the lab ambient conditions where the measurements were made. Similar observations are obtained in the s-velocity vs porosity plots (Figure 10).

Another important observation is the increase in the acoustic anisotropy with decreasing porosity. This is attributed to the increasing alignment of clay minerals with compactions. Clays have intrinsic anisotropies and increased parallel orientation increases the anisotropy as a whole. The orientation of clays also controls the permeability anisotropy of shales. Clennell et al. (1999) reported permeability anisotropy in clays (Kaolinite, CaMontmorillonite and silty clay from ODP) and related to the degree of particle orientation due to compaction. Understanding the controls of acoustic velocities and permeability for the clays will help us predict permeability anisotropy from anisotropic seismic velocities.

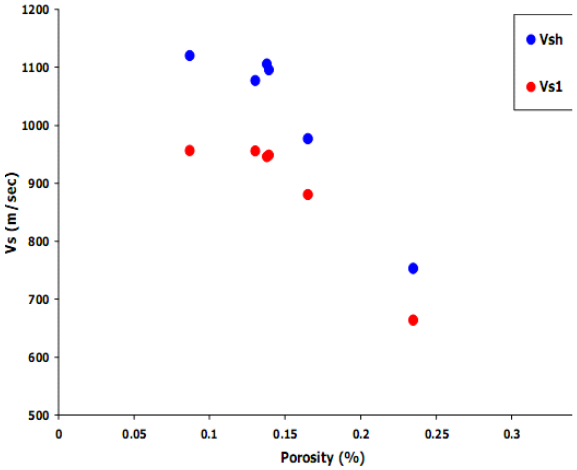

Figure 6 S-wave velocities as a function of porosity.

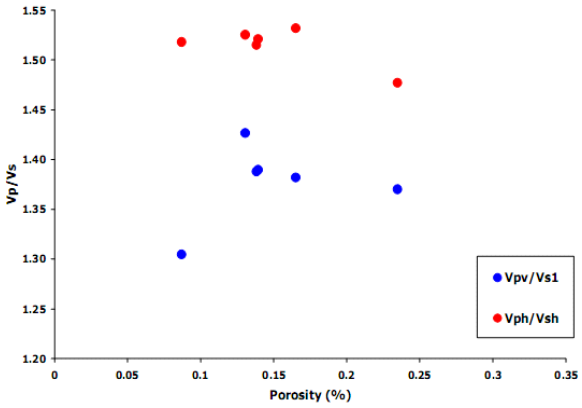

Figure 7. Vp/Vs as a function of porosity. Note that the Vph/Vsh is relatively insensitive to porosity changes.

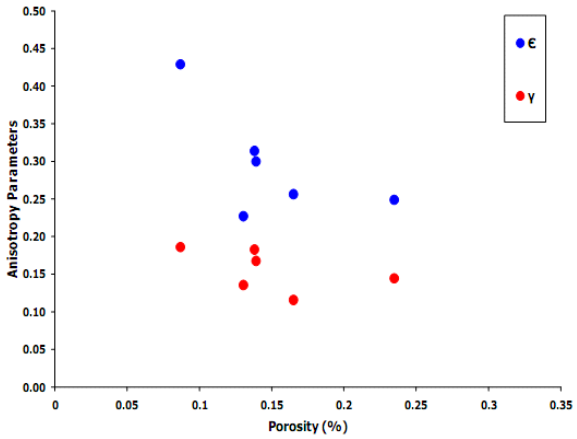

Figure 8. Anisotropic parameters as a function of porosity

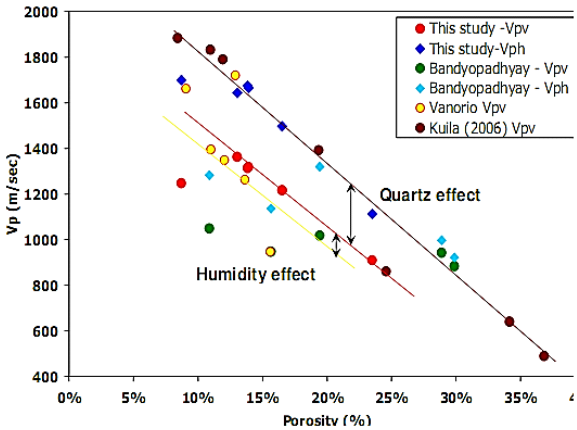

Figure 9: Comparison of P-wave data on dry samples reported in the literature. The circles indicate Vpv and the diamonds are the Vph. Note the trendlines drawn are not fitted regressive linear correlations but is shown to compare the data sets. Kuila et al. reported velocities are higher compared to this study owing to the presence of quartz in the former's case. The difference between Vanorio's data can be attributed to humidity difference.

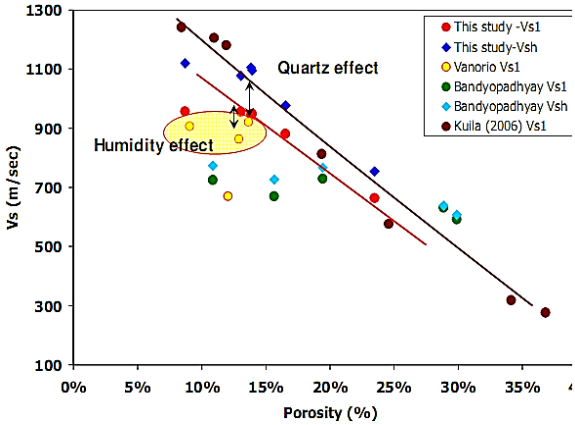

Figure 10. Comparison of S-wave data on dry samples reported in the literature. Same observations as obtained in the previous figure

Refernces

A. U. Dogan et al., "Baseline studies of the Clay Minerals Society source clays: specific surface area by the Brunauer Emmett Teller (BET) method" , Clays and Clay Minerals, Volume 54, Number 1, February 2006 , pp. 62-66(5)

C. G. Schull, "The Determination of Pore Size Distribution from Gas Adsorption Data," Journal of the American Chemical Society, vol. 70, pp. 1405-1410 1948.

J. B. Condon, Surface area and porosity determinations by physisorption :measurements and theory, 1st ed. ed. Amsterdam ;Boston: Elsevier,, 2006.

K. Bandyopadhyay, et al., "Elastic anisotropy of clay," SEG Technical Program Expanded Abstracts, vol. 27, pp. 18351839, 2008.

M.B. Clennell et al.,, "Permeability anisotropy of consolidated clays ", from A. C. Aplin, et al.., Muds and mudstones : physical and fluid-flow properties. London: Geological Society, Special Publications, vol. 158, pp. 7996, 1999.

P. D. Schettler, et al.., "Gas Storage and Transport in Devonian Shales," SPE Formation Evaluation, vol. 4, pp. 371-376, 1989.

R. M. Bustin, et al., "Impact of Shale Properties on Pore Structure and Storage Characteristics," presented at the SPE Shale Gas Production Conference, Fort Worth, Texas, USA, 2008.

R. T. Ewy and E. K. Morton, "Shale Swelling Tests Using Optimized Water Content and Compaction Load," presented at the SPE Western Regional Meeting, San Jose, California, 2009.

T. Vanorio, et al., "Elastic properties of dry clay mineral aggregates, suspensions and sandstones," Geophysical Journal International, vol. 155, p. 319, 2003

T.J. Katsube, et al., "Shale Pore Structure Evolution and its Effect on Permeability,"in Symposium Volume III of 33 Annual Symposium of the Society of Professional Well Log Analysts ,Society of Core Analysts Preprints, SCA-6214, vol. 3, pp. 1-24, 1992.

U. Kuila, et al., "Measuring and modeling the elastic moduli of clay minerals," SEG Technical Program Expanded Abstracts, vol. 25, pp. 1893-1897, 2006.

Table 2: BET surface area and BJH pore volume obtained from the gas adsorption experiment

	NaM100-pw-US	NaM100-pw-Se	NaM100-13K
BET Surface Area m^2/g	30.7038	36.7260	35.3781
BJH Adsorption cum. pore vol. (17 Å -3000 Å) cm^3/g	0.09294 (17.6%)	0.12647 (22.5%)	0.06945 (13.7%)
BJH Desorption cum. pore vol. (17 Å -3000 Å) cm^3/g	0.09723 (18.3%)	0.12954 (23.0%)	0.07891 (15.3%)

Table1: Porosity, bulk density and grain density of cold pressed samples

Sample	Axial Load	Bulk Volume	Weight	Bulk Density	Grain Density	Porosity	Comments
	Psi	Cc	gm	g/cc	g/cc	%	
NaM100-14k-1	14000	12.07	23.931	1.98	2.3	13.81%	perfect cube, clays sieved through 400 mesh
NaM100-14k	14000	10.49	22.080	2.10	2.3	8.52%	edge broken
NaM100-12k-1	12000	12.38	24.497	1.98	2.3	13.94%	edge broken, clays sieved through 400 mesh
NaM100-12K	12000	12.61	25.220	2.00	2.3	13.04%	edge broken
NaM100-10k	10000	12.64	24.255	1.92	2.3	16.57%	edge broken
NaM100-6k	6000	11.75	20.710	1.76	2.3	23.39%	edge broken